Quantum Kicked Rotor in a Highly Inhomogeneous Magnetic Field

D. Mašović*

Vinča Institute of Nuclear Sciences, Laboratory for Theoretical and Condensed Matter Physics, 11001 Belgrade, P.O.Box 522, Serbia

Received: 10.07.2024 & Accepted: 26.08.2024

Doi: 10.12693/APhysPolA.146.295 *e-mail: dragmasovic@gmail.com

A new model of a spin-$\frac{1}{2}$ quantum kicked rotor coupled with a highly inhomogeneous magnetic field is proposed. The model is mapped into the appropriate tight-binding equations, and then the problem of localization is considered. The introduced tight-binding model is verified by calculating the localization length for the appropriate quasi-energy states. In particular, it is shown that the functional form of the spin-dependent term in kicking potential is exclusively responsible for the growth of the localization length with an increase in the magnitude of the magnetic field. The growth is more pronounced if the inhomogeneity of the magnetic field is greater. Thus, quasi-extended states appear as a consequence of strongly conspicuous inhomogeneity, and they exhibit nonstandard localization properties. Their existence is also shown by calculating the appropriate inverse participation ratio and pair-correlations. Therefore, some kind of "localization–delocalization" transition is possible here. This has been demonstrated as well by following the time evolution of the wave packet in the angular momentum space, assuming increasing inhomogeneity. For extremely large inhomogeneity, dynamical localization is destroyed. The model proposed here can serve as an assessment simulator for the induced electric dipole moment in a hydrogen-like atom, assuming the existence of anisotropy.

topics: quantum chaos, kicked rotor, inhomogeneous magnetic field, dynamical localization

1. Introduction

Quantum mechanical periodically driven systems, most often represented by the kicked rotor (KR), have been lengthily examined regarding chaos and quantum chaos (see for example [1–5]). It has been registered that unbounded diffusion as a characteristic of deterministic chaos in classical systems is suppressed in the quantum ones. This phenomenon is known as dynamical localization. The appropriate mechanism is similar to the Anderson localization in disordered solids [6]. Thus, for large kick strengths, the effects such as quantum resonance and dynamical localization are established. More precisely, dynamical localization means localization in momentum space, while Anderson localization implies localization in a spatially disordered medium. Thus, the physics of Anderson localization is highly dependent on the dimensions of the systems. While for 1D and 2D the mentioned similarity is considered established (see for example [7]), the 3D case is particularly interesting, especially in connection with localization–delocalization transitions. Examinations of this similarity still attract attention [8, 9].

The quantum kicked rotor (QKR) for a spin-$\frac{1}{2}$ particle was introduced by Scharf in [10]. There, the occurring dynamical localization was studied in the resonant regime. Further, the QKR model augmented by a spin-$\frac{1}{2}$ in a homogeneous and inhomogeneous magnetic field was examined in [11, 12]. At that time, a very interesting problem was the importance of time-reversal symmetry in QKR models with dynamical localization in relation to the localization length (LOC) changes [13, 14]. Thus, it was shown that the breaking of the conventional time-reversal (anti-unitary) symmetry by magnetic field has no influence on LOC changes.

In our times, interest in KR exists due to its recent experimental realizations in atom optics [15, 16], especially among the group of authors of works [17–20]. Moreover, it seems that, for now, the most important application of the quantum kicked rotor can be in molecular physics for rotational excitations of diatomic molecules. It is

confirmed by the appropriate experimental results [21, 22]. More recently, theoretical KR has also been proposed for application in attosecond spectroscopy [23].

In particular, assuming that dynamical localization can be related to Anderson localization of disordered systems, through a mapping of the Floquet eigenvalue problem (time periodic problem for KR) on a tight-binding problem with a potential periodic in space, the LOC changes of QKR can be very interesting in solid state physics as well. Therefore, we propose here the appropriate model of spin-$\frac{1}{2}$ QKR in a highly inhomogeneous magnetic field, and we consider its mapping to the appropriate tight-binding equations. Then, the localization problem will be analyzed within the framework of this second approach.

Nevertheless, the most interesting problem will be to consider whether magnetic field inhomogeneity in general can cause transitions from localized to quasi-extended states. The spreading of the wave packet in the angular momentum space is expected, so some kind of "localization–delocalization" transition seems possible here in the ordinary one-dimensional QKR [8]. This will also be considered as an important problem in this paper.

The organization of the rest of the paper is as follows. In Sect. 2, our model of the spin-$\frac{1}{2}$ QKR in a highly inhomogeneous magnetic field and the appropriate tight-binding model are given. In Sect. 3, the results are presented, and finally, the conclusion is given in Sect. 4.

2. Model

A simple KR model suitable for the physical performance of the KR is proposed in [11, 12]. A spin-$\frac{1}{2}$ electron is in an impenetrable ring located in the x–y plane. It simulates a rotor while the kicking electric field is along the x-axis. The kicking magnetic field is also assumed along the same axis, making the magnetic field inhomogeneous across the ring.

The appropriate Schrödinger equation in the velocity gauge is

$$\mathrm{i}\frac{\partial}{\partial t}\begin{pmatrix}\Psi_1\\ \Psi_2\end{pmatrix} = \Big[-\frac{\tau}{2}\frac{\partial^2}{\partial\theta^2}\mathbb{1} + k\cos(\theta)\sum_{n'=-\infty}^{\infty}\delta(t-n')\mathbb{1} + H\cos(n\theta)\sigma_x\sum_{n'=-\infty}^{\infty}\delta(t-n')\Big]\begin{pmatrix}\Psi_1\\ \Psi_2\end{pmatrix}, \tag{1}$$

where τ and k are the standard parameters of a spinless QKR [6], H corresponds to the magnitude of the θ-dependent magnetic field, $\mathbb{1}$ is the (2×2) unit matrix, and σ_x is the Pauli spin matrix. Here, we assume integer $n \geq 1$. Since the appropriate Hamiltonian is periodic in time, the spinor in (1) has the form

$$\begin{pmatrix}\Psi_1\\ \Psi_2\end{pmatrix} = \mathrm{e}^{-\mathrm{i}\omega t}\frac{1}{\sqrt{2\pi}}\sum_{m=-N}^{N}\mathrm{e}^{\mathrm{i}m\theta}\begin{pmatrix}u_m^{1-}\\ u_m^{2-}\end{pmatrix}, \tag{2}$$

where ω is the quasi-energy. In order to study the quantum behavior of the model, we must solve the eigenvalue problem

$$\sum_{m=-N}^{N}\mathrm{e}^{-\mathrm{i}\frac{\tau}{2}n^2}\begin{pmatrix}\langle nAm\rangle & \langle n\mathrm{i}Bm\rangle\\ \langle n\mathrm{i}Bm\rangle & \langle nAm\rangle\end{pmatrix}\begin{pmatrix}u_m^{1-}\\ u_m^{2-}\end{pmatrix} = \mathrm{e}^{-\mathrm{i}\omega}\begin{pmatrix}u_m^{1-}\\ u_m^{2-}\end{pmatrix}, \tag{3}$$

where

$$A = \mathrm{e}^{-\mathrm{i}k\cos(\theta)}\cos(H\,\cos(n\theta)) \tag{4}$$

and

$$B = -\mathrm{e}^{-\mathrm{i}k\cos(\theta)}\sin(H\,\cos(n\theta)). \tag{5}$$

Then, under the appropriate orthogonal transformation

$$O\begin{pmatrix}\langle nAm\rangle & \langle n\mathrm{i}Bm\rangle\\ \langle n\mathrm{i}Bm\rangle & \langle nAm\rangle\end{pmatrix}\tilde{O}, \tag{6}$$

where

$$O = \frac{1}{\sqrt{2}}\begin{pmatrix}1 & 1\\ 1 & -1\end{pmatrix} \tag{7}$$

and $\tilde{O}$ is the transposed matrix, two independent eigenvalues problems are obtained

$$\sum_{m=-N}^{N}\Big(\mathrm{e}^{-\mathrm{i}\frac{\tau}{2}n^2}F_{nm}^{q} - \mathrm{e}^{-\mathrm{i}\omega}\delta_{nm}\Big)w_m^{q-} = 0, \tag{8}$$

where

$$F_{nm}^{q} = \frac{1}{2\pi}\int_0^{2\pi}\mathrm{d}\theta\;\mathrm{e}^{\mathrm{i}(m-n)\theta}\mathrm{e}^{-\mathrm{i}(k\cos(\theta)\pm H\cos(n\theta))} \tag{9}$$

and

$$w_m^{q-} = \frac{u_m^{1-} \pm u_m^{2-}}{\sqrt{2}}. \tag{10}$$

In (8)–(10), index $q = 1$ implies sign $(+)$ and $q = 2$ sign $(-)$, respectively. Integral (9) can be solved analytically, and the corresponding solution by default $r = m - n$ is

$$F_r^q = J_0(H)J_r(k)(-1)^r\mathrm{i}^r + \sum_{s=2p>0}^{\infty}J_s(H)\Big[J_{r+sn}(k) + J_{r-s\,n}(k)\Big](-1)^r\mathrm{i}^{r+s(n+1)} \pm \sum_{s=2p+1>0}^{\infty}(-1)^{r+sn+1}J_s(H) \times\Big[W_{r+sn}^1(k) + (-1)^n W_{r-s\,n}^1(k) + \mathrm{i}\Big(W_{r+sn}^2(k) + (-1)^n W_{r-s\,n}^2(k)\Big)\Big]\mathrm{i}^{r+s(n+1)}, \tag{11}$$

where J are Bessel functions of the first kind. Functions W^1 and W^2 in (9) are determined as

$$\begin{cases} W_l^1 = 0 \quad \text{for} \quad n = 2p+1, \\ W_l^1 = \frac{2}{\pi}\cos\left(\frac{n\pi}{2}\right)\left[\frac{(-1)^j n J_0(k)}{l}\delta_{l,(2j+1)n} + \sum_{m=m_1}^{\infty}\frac{(-1)^m J_{(2m+1)n-l}(k)}{2m+1} + \sum_{m=m_2}^{\infty}\frac{(-1)^m J_{(2m+1)n+l}(k)}{2m+1}\right] \\ \qquad \text{for} \quad n = 2p \quad \text{and} \quad l = 2i, \\ W_l^1 = -\frac{2}{\pi}\cos\left(\frac{n\pi}{2}\right)\left[\sum_{m=m_1}^{\infty}\frac{(-1)^m J_{(2m+1)n-l}(k)}{2m+1} - \sum_{m=m_2}^{\infty}\frac{(-1)^m J_{(2m+1)n+l}(k)}{2m+1}\right] \\ \qquad \text{for} \quad n = 2p \quad \text{and} \quad l = 2i+1, \end{cases} \tag{12}$$

and

$$\begin{cases} W_l^2 = 0 \quad \text{for} \quad n = 2p, \\ W_l^2 = -\frac{2}{\pi}\sin\left(\frac{n\pi}{2}\right)\left[\sum_{m=m_1}^{\infty}\frac{J_{(2m+1)n-l}(k)}{2m+1} + \sum_{m=m_2}^{\infty}\frac{J_{(2m+1)n+l}(k)}{2m+1}\right] \\ \qquad \text{for} \quad n = 2p+1 \quad \text{and} \quad l = 2i, \\ W_l^2 = \frac{2}{\pi}\sin\left(\frac{n\pi}{2}\right)\left[\frac{n J_0(k)}{l}\delta_{l,(2j+1)n} + \sum_{m=m_1}^{\infty}\frac{J_{(2m+1)n-l}(k)}{2m+1} - \sum_{m=m_2}^{\infty}\frac{J_{(2m+1)n+l}(k)}{2m+1}\right] \\ \qquad \text{for} \quad n = 2p+1 \quad \text{and} \quad l = 2i+1. \end{cases} \tag{13}$$

Parameters m_1 and m_2 in (12) and (13) are obtained as the first integers for which the following relations are satisfied:

1. n odd and l odd or n even and l even, therefore for $s = 1, 2, 3, \ldots$, one has
$$\frac{2s+l}{n} = \ldots, 2m_1+1, \ldots,$$
$$\frac{2s-l}{n} = \ldots, 2m_2+1, \ldots;$$
2. n odd and l even or n even and l odd, therefore for $s = 0, 1, 2, 3, \ldots$, one has
$$\frac{2s+1+l}{n} = \ldots, 2m_1+1, \ldots,$$
$$\frac{2s+1-l}{n} = \ldots, 2m_2+1, \ldots.$$

Functions W^1 and W^2 have the following properties

$$W_l^1(-k) = (-1)^l W_l^1(k), \tag{14}$$

$$W_{-l}^1(k) = (-1)^l W_l^1(k), \tag{15}$$

$$W_l^2(-k) = (-1)^{l+1} W_l^2(k), \tag{16}$$

and

$$W_{-l}^2(k) = (-1)^l W_l^2(k). \tag{17}$$

The solution of the integral (9) and previous analytical formulas obtained on the basis of extensive mathematics seem very complicated. To make everything more convincing, we give some of the test results concerning the solutions of the integral (9) in the Appendix.

It should be pointed out that the case for $n = 1$ is specific. Then, $W_l^1 = 0$ and $W_l^2 = E_l$. Let us emphasize that in [12], the appropriate analytical solution for $n = 1$ was obtained in a different way. Thus, a systematic step-by-step comparison in both derivations led to the following two key relations

- for $s = 2p$

$$\sum_{s=-\infty}^{\infty} J_s(H) J_{r+s}(k) = \frac{J_r(k+H) + J_r(k-H)}{2}, \tag{18}$$

and

- for $s = 2p+1$

$$\mp \sum_{s=-\infty}^{\infty} J_s(H) E_{r+s}(k) = \pm \frac{E_r(k+H) - E_r(k-H)}{2}, \tag{19}$$

where

$$E_r(z) = \frac{1}{\pi}\int_0^{\pi} \mathrm{d}\theta \ \sin(r\theta - z\sin(\theta)) \tag{20}$$

is the Weber function [24] with properties

$$E_r(-z) = (-1)^{r+1} E_r(z) \tag{21}$$

and

$$E_{-r}(z) = (-1)^r E_r(z). \tag{22}$$

Thus, it can be shown that F_r^q also has the following simple and compact form

$$F_r^q = (-\mathrm{i})^r \left[\frac{J_r(k+H) + J_r(k-H)}{2} \pm \mathrm{i}\frac{E_r(k+H) - E_r(k-H)}{2}\right]. \tag{23}$$

In particular, we also checked that the matrix elements in (8) obtained in both ways are in complete agreement.

It turns out that the unitary matrix in (8) is the band matrix for $n \geq 1$ with $b \sim k + H$, where b is the band half-width. Therefore, outside the band matrix, elements decay exponentially. Thus, it is to be expected that by solving the eigenvalue problem (8), exponentially localized states appear [25].

Previously, it was mentioned that there is an analogy between the dynamical localization of the QKR and Anderson localization in disordered solids. Thus, on that basis, it is possible to map the QKR problem on the tight-binding model. Then, the characteristics of quasi-energy states are further investigated within this model. There are two different mapping methods. The first one, suggested by Gremel, Prange, and Fishman [6], gives two coupled tight-binding equations. Note that for $H = 0$, the values of the parameter k in such an approach must be $k < \pi$, which is the disadvantage of this method. A different mapping was proposed by Shepelyansky [26, 27], and that procedure is appropriate for greater values of the parameter k. Here, we will generalize Shepelyansky's mapping procedure to include spin and then study localization by means of transfer matrices. Thus, the appropriate derivation leads to the following general results for tight-binding equations

$$\sum_{r=-b}^{b} \left[X_r \sin\left(\varphi_l - r\frac{\pi}{2}\right) \pm Y_r \cos\left(\varphi_l - r\frac{\pi}{2}\right) \right] w_{l+r}^{q-} = 0. \tag{24}$$

Assuming from now on the pseudo-random transfer matrix calculation, φ_l in (24) is

$$\varphi_l = \frac{\omega - \tau\, l^2/2}{2}. \tag{25}$$

In particular, we have

$$X_r = J_0\Big(\frac{H}{2}\Big) J_r\Big(\frac{k}{2}\Big) + \sum_{s=2p>0}^{\infty} \cos\Big((n+1)s\frac{\pi}{2}\Big) J_s\Big(\frac{H}{2}\Big) \times \Big[J_{r+sn}\Big(\frac{k}{2}\Big) + J_{r-s\,n}\Big(\frac{k}{2}\Big) \Big], \tag{26}$$

and further for odd n values

$$Y_r = \sum_{s=2p+1}^{\infty} \cos\Big((n+1)s\frac{\pi}{2}\Big) J_s\Big(\frac{H}{2}\Big) \times \Big[W_{r+sn}^2\Big(\frac{k}{2}\Big) + (-1)^n W_{r-s\,n}^2\Big(\frac{k}{2}\Big) \Big], \tag{27}$$

while for even n values

$$Y_r = -\sum_{s=2p+1>0}^{\infty} \sin\Big((n+1)s\frac{\pi}{2}\Big) J_s(\frac{H}{2}) \times \Big[W_{r+sn}^1\Big(\frac{k}{2}\Big) + (-1)^n W_{r-s\,n}^1\Big(\frac{k}{2}\Big) \Big]. \tag{28}$$

We note that the case $n = 1$ is specific so that simple and compact formulas are also valid, i.e.,

$$X_r = \frac{J_r(\frac{k+H}{2}) + J_r(\frac{k-H}{2})}{2} \tag{29}$$

and

$$Y_r = \frac{E_r(\frac{k+H}{2}) + E_r(\frac{k-H}{2})}{2}. \tag{30}$$

3. Results

In order to estimate dynamical localization in our model, we will apply the pseudo-random transfer matrix method [3], assuming the tight-binding equations (24). Thus, Fig. 1 shows the dependence of the appropriate transfer matrix results $\langle \mathrm{LOC} \rangle$, obtained by averaging over ten different initial conditions in each of the calculations, on the magnitude of the magnetic field H for $k = 10$ and for $n = 1, 2$, and 3. The main feature is the anomalous and continuous growth of $\langle \mathrm{LOC} \rangle$ with an increase in H as well as with the degree of inhomogeneity of the magnetic field. More precisely, the best fit suggests polynomial (of the second degree) dependence on H for greater inhomogeneity. For example, for the curve 'b' in Fig. 1, we have

$$\langle \mathrm{LOC} \rangle = 18.18182 + 3.64848\, H + 0.87879\, H^2. \tag{31}$$

It is a different form of $\langle \mathrm{LOC} \rangle$ dependence than for the spinless QKR [26, 27]. We also note that the random transfer matrix gives a slightly slower growth of $\langle \mathrm{LOC} \rangle$ with H.

Figures 2–3 show examples of dynamical localization for some quasi-energy states and for the given values of model parameters. These results are obtained by solving the eigenvalue problem (8). The corresponding LOC estimates are also given. The parity operator [23] now has the unique form $I = R_x^{\mathrm{o}} R_x^{\mathrm{s}}$, where R_x is a rotation by π about the x-axis and R_x^{o}, and R_x^{s} are the orbital and spin parts, respectively. Thus, the quasi-energy states can be either even or odd. It is evident that exponential localization is noticeable in all examples. Note that the odd state in Fig. 2 is symmetrical with respect to coordinate origin in $m = 0$. Then, we have $\mathrm{mod}(w_0^{1-}) = 0$ and $\ln(\mathrm{mod}(w_0^{1-})) \to -\infty$. In this way, the odd state can be immediately recognized in computations. We always have one peak

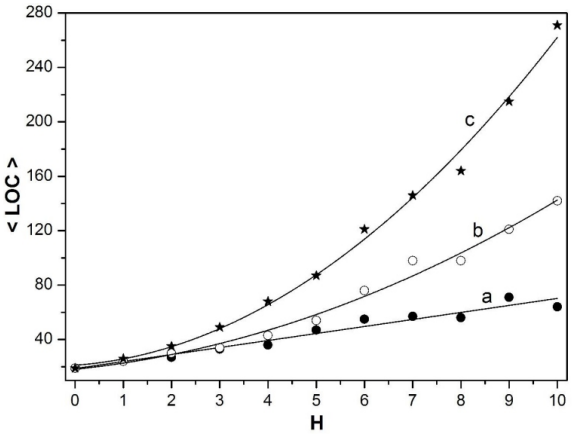

Fig. 1. Pseudo-random transfer matrix results: $\langle \mathrm{LOC} \rangle$ as a function of H for $k = 10$ and $n = 1$ (curve a), $n = 2$ (curve b), and $n = 3$ (curve c).

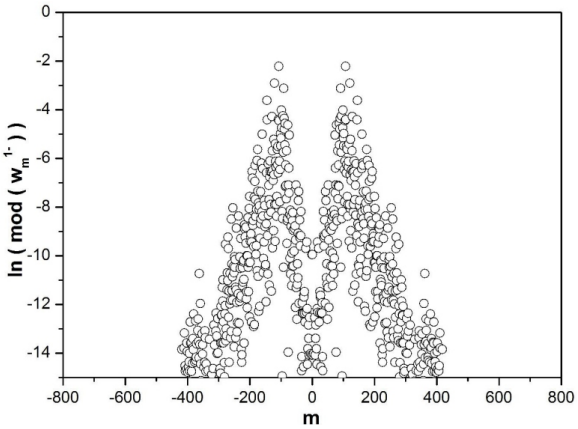

Fig. 2. Dynamical localization in angular momentum space for $n = 1$, $\tau = 1$, $k = 10$, and $H = 10$. Results $\ln(\mathrm{mod}(w_m^{1-}))$ as a function of m for the chosen odd state are obtained by solving (28). The estimated LOC = 66.

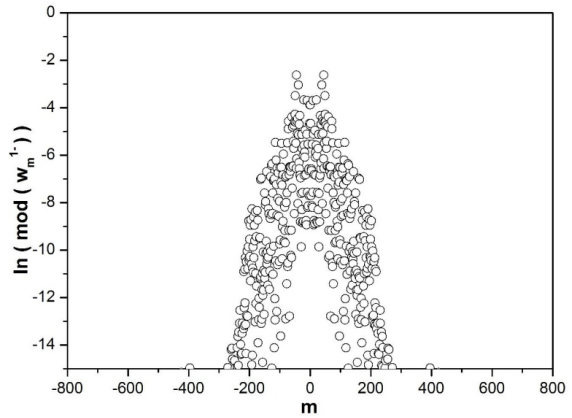

Fig. 3. Dynamical localization in angular momentum space for $n = 2$, $\tau = 1$, $k = 10$, and $H = 6$. Results $\ln(\mathrm{mod}(w_m^{1-}))$ as a function of m for the chosen even state are obtained by solving (28). The estimated LOC = 57.

symmetric with respect to the coordinate origin. If the peak is centered near the coordinate origin at m_0, an exponential tail is considered for $m > m_0$ or due to symmetry for $-m < -m_0$. Let us note that the asymptotic decay rate of the quasi-energy eigenfunctions here has a form

$$w_m^{1-} \sim C\, w_{m_0}^{1-} \exp\Big(-\frac{m-m_0}{\mathrm{LOC}}\Big), \tag{32}$$

where C is a constant. The unique value of $\ln(C)$ is chosen so that the transfer matrix result $\langle \mathrm{LOC} \rangle$ fits the appropriate individual results for LOC for different quasi-energy states. It was also numerically verified for the appropriate spinless tight-binding model [26, 27]. Thus, $\langle \mathrm{LOC} \rangle$ calculated by the transfer matrix method is a satisfactory estimate of localization length for the given values of model parameters as mean. It also gives credibility to the tight-binding model proposed here.

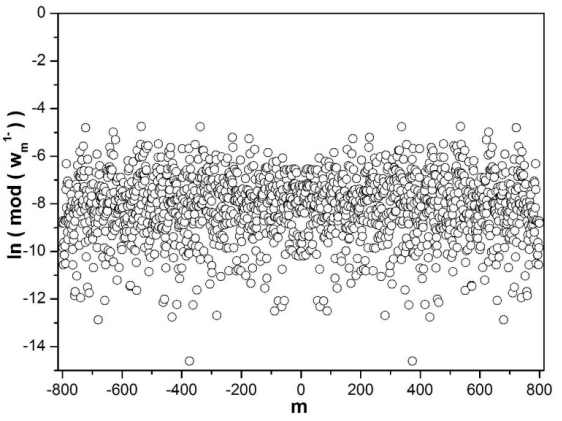

Fig. 4. Quasi-extended even state in angular momentum space for $n = 50$, $\tau = 1$, $k = 10$, and $H = 6$. Results $\ln(\mathrm{mod}(w_m^{1-}))$ as a function of m are obtained by solving (28).

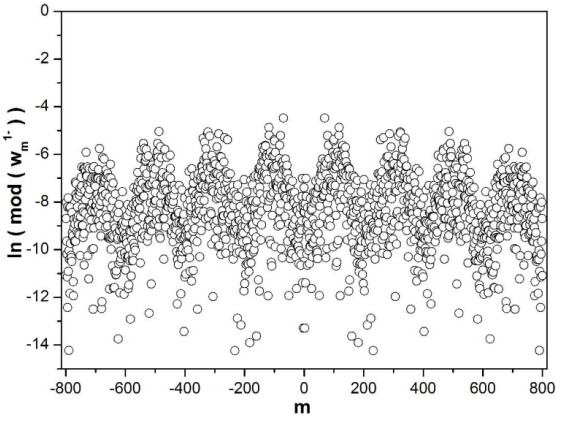

Fig. 5. Quasi-extended even state in angular momentum space for $n = 100$, $\tau = 1$, $k = 10$, and $H = 6$. Results $\ln(\mathrm{mod}(w_m^{1-}))$ as a function of m are obtained by solving (28).

With an increase in n, the spreading of the wave packet in the angular momentum space becomes more intense. For sufficiently large n, dynamical localization still exists, but the LOC exceeds the half-width of the wave packet, as shown in Fig. 4. Therefore, we will denote those specific states as quasi-extended states. Of course, here, the magnitude of the magnetic field is considered constant. It is evident that LOC for quasi-extended states increases with increasing inhomogeneity. We emphasize that the transfer matrix is not applicable, assuming quasi-extended states. The minimal positive Lyapunov exponent is then in the range of numerical noise, and the uncertainty of the final results is unacceptable. In particular, Fig. 5 shows the results for $n = 100$. Here, the quasi-extended state has an unusual form. Such a form begins to appear for $n \gtrsim 85$. Thus, this "oscillatory" form means that dynamical localization (and exponential localization) is destroyed.

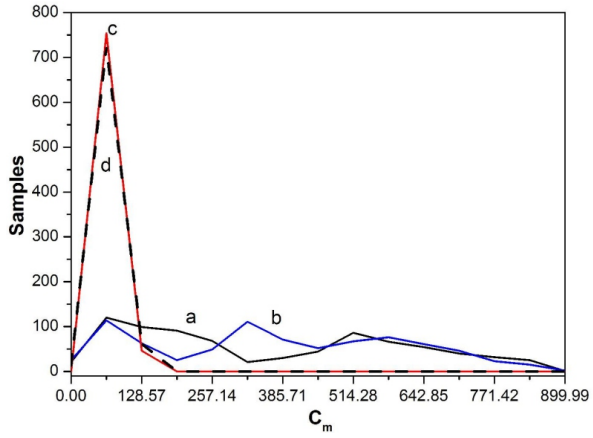

Fig. 6. Distributions of pair-correlations C_m for $r = 1$ assuming 800 samples: (a) $n = 1$ and $H = 10$, (b) $n = 2$ and $H = 6$, (c) $n = 50$ and $H = 6$. (d) Simulated appropriate extended state. The other parameters are $k = 10$, $\tau = 1$, and sign $(+)$.

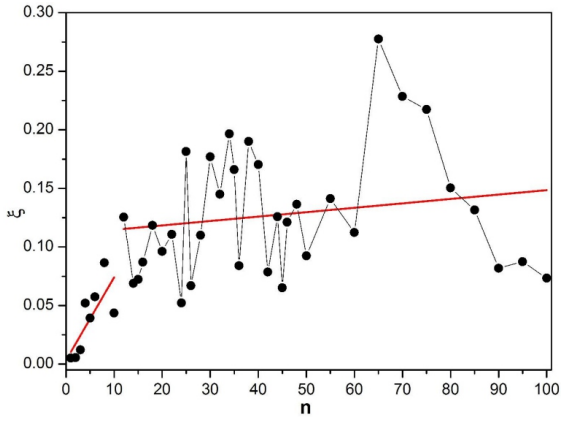

Fig. 7. Inverse participation ratio ξ according to n. Other parameters are $k = 10$, $H = 6$, $\tau = 1$, and sign $(+)$.

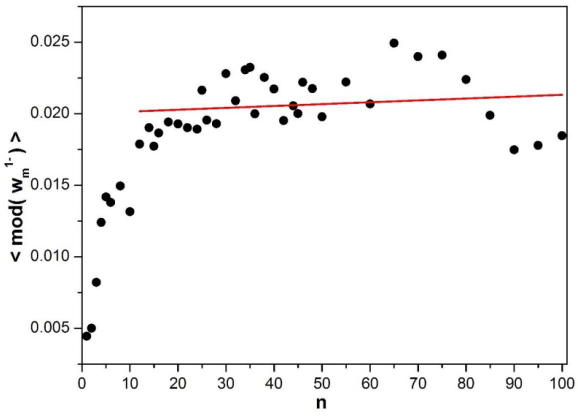

Fig. 8. The average values of w_m^{1-} according to n. Other parameters are $k = 10$, $H = 6$, $\tau = 1$, and sign $(+)$.

The difference between the quasi-extended states and quasi-energy states with the standard localization properties can be seen by calculating the pair-correlations

$$C_m = \ln\left(w_m^{1-}\right) \ln(w_{m+r}^{1-}). \tag{33}$$

Thus, for $r = 1$ and $m = 0, 1, 2, \ldots, N-1$, the appropriate histogram is shown in Fig. 6. The difference in the distributions of C_m for the quasi-extended state, marked with the letter 'c', and those with standard localization, marked with the letters 'a' and 'b', for small n is clearly visible. We emphasize that quasi-extended states always have such prominent peaks in the initial part of the histogram. It means that the vast majority of pairs $\ln(w_m^{1-})$ separated by a certain distance r have close values of C_m, which is a sign of "delocalization." Then, we also simulated the appropriate extended state in a simple way. Namely, assuming random numbers $x_m \in [0, 1]$, we consider the following function

$$y_m = c_1 x_m + c_2 + \langle \ln\left(w_m^{1-}\right)\rangle, \tag{34}$$

where $\langle \ln(w_m^{1-})\rangle$ is the corresponding mean value of $\ln(w_m^{1-})$ and c_1, c_2 are estimated constants, in order to obtain a more complete agreement with the sizes $\ln(w_m^{1-})$. In this way, the considered quasi-extended state and its suitable extended state can be compared. The calculated pair-correlations C_m for (34) are shown in Fig. 6, marked with the letter 'd'. The agreement between curve c and curve d is noticeable. Thus, "delocalization" and nonstandard localization properties of quasi-extended states are confirmed. Our check with other appropriate data shows that the results are similar to those in Fig. 6. It can also be seen that characteristic peaks for quasi-extended states appear for $n > 10$. Similar results are obtained for $r = 2$. We emphasize that the comparison of the mean distribution for standard quasi-extended states ($10 < n < 85$) with the one for $n = 100$ does not give anything special. The "delocalization" is only slightly less pronounced. Thus, the corresponding distribution for $n = 100$ is practically indistinguishable, from the point of view of "delocalization", from those for standard quasi-extended states.

In order to further estimate the appearance of quasi-extended states, we will also calculate the inverse participation ratio [28, 29]

$$\xi = \frac{1}{\mathrm{N}+1} \frac{\sum_m (w_m^{1-})^2}{\sum_m (w_m^{1-})^4}, \tag{35}$$

assuming $m \in [0, N]$. Therefore, $\xi \to 0$ indicates localization. The results for the appropriated range of n are shown in Fig. 7. Then, for the initial values n, linear growth of ξ is noticeable, which is expected since it corresponds to the previously discussed increase in LOC. In particular, we note that for $n > 10$ it is evident that ξ oscillates around the value $\xi \sim 0.12$. It is a sign of the presence of quasi-extended states. Thus, the significant values

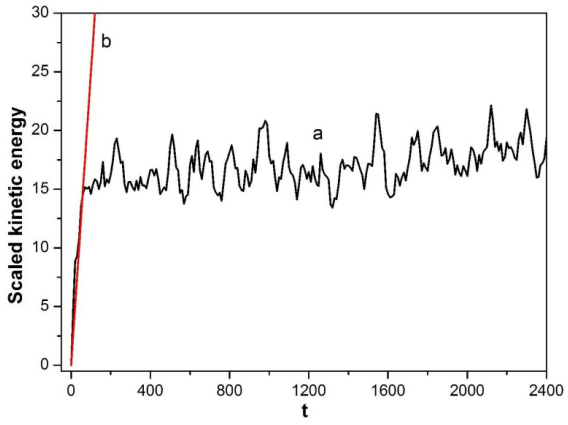

Fig. 9. Scaled kinetic energy (divided by 100) in time corresponding to (a) quantum case, (b) classical case for $n = 1$. Other parameters are $k = 10$, $H = 6$, $\tau = 1$, and sign $(+)$. Shown up to $t = 2400$.

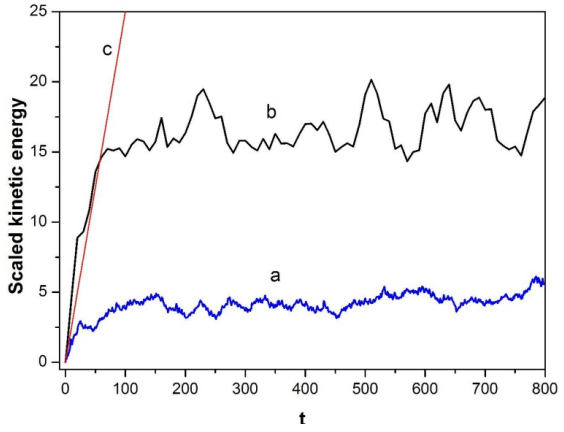

Fig. 10. Scaled kinetic energy in time corresponding to (a) quantum-spinless case, (c) classical case. Other parameters are $k = 10$, $H = 6$, $\tau = 1$, and sign $(+)$. Results are shown up to $t = 800$.

of w_m^{1-} appear now in the whole range of m. Specifically, their distribution depends both on n and the selected quasi-energy state. As a consequence, the oscillations appear. As an additional argument, we note that the presence of quasi-extended states for $n > 10$ is also obvious when calculating the average value $\langle w_m^{1-} \rangle$ as a function of n (see Fig. 8). Then, for fitting in this range, we can assume $\langle w_m^{1-} \rangle \sim 0.02$ as a sign for the existence of quasi-extended states.

The classical KR assuming a fully developed chaos shows a linear growth of kinetic energy. It is also well known that the quantum effects tend to suppress this diffusion due to the mechanism of dynamical localization [1]. Thus, we assume here the wave packet, initially located at 0 site in angular momentum space, and we will follow its time evolution for the different values of n, keeping the other model parameters in the evolution operator the same. Figure 9 shows the results for $n = 1$. It can

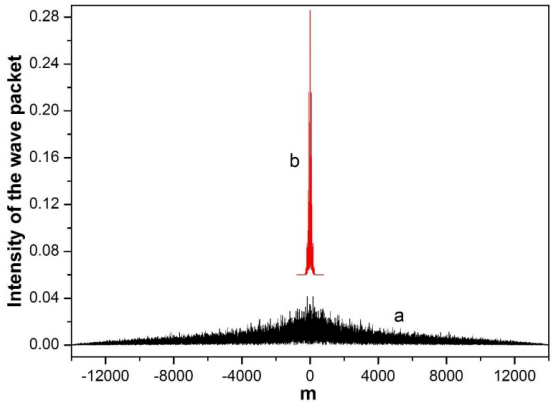

Fig. 11. Intensity of the wave packet in angular momentum space: (a) $n = 20$, (b) spinless, raised for $+0.06$. Other parameters are $k = 10$, $H = 6$, $\tau = 1$, and sign $(+)$.

be seen that at the beginning, with some minor deviations, there is agreement between classical and quantum growth of kinetic energy. After that, the suppression of diffusion begins. Here, we emphasize that the a curve in Fig. 9 does not change with the increase in size of the numerical basis. Also, the final form of the wave packet, at $t = 6000$, is not dependent on the basis size. The deviation between classical and quantum initial growth becomes more and more pronounced with a further increase in n. Then, it is evident that there is no longer any similarity between the quantum and classical growth. For $n = 20$, assuming quasi-extended states, it should be pointed out that the sign of "delocalization" assumes

$$\text{Energy}_{kin}^{\text{deloc}} \gg \text{Energy}_{kin}^{\text{spinless}}, \tag{36}$$

where $\text{Energy}_{kin}^{\text{spinless}}$ is the kinetic energy for the corresponding spinless QKR (see Fig. 10). Note that in Fig. 10 only a and c curves have the appropriate agreement for the first values of t [1]. Nevertheless, "delocalization" can also be seen by comparing the width of the corresponding final wave packet with the spinless one. Namely, the width of the spinless wave packet is much smaller (see Fig. 11).

In particular, we will examine the similarity between the quantum and classical initial growth of the kinetic energy noticeable in Figs. 9 and 10 and mentioned previously for $n = 1$. Thus, we will compare the following functions

$$y_1(\theta) = k\cos(\theta) + H\big|\cos(n\theta)\big| \tag{37}$$

and

$$y_2(\theta) = \left(k + \frac{H}{2}\right)\cos(\theta), \tag{38}$$

for the values of the parameters $k = 10$ and $H = 6$ and for different values of n. The function (37) corresponds to the exponent in the evolution operator supposing spin and inhomogeneous magnetic field, while (38) corresponds to the exponent for

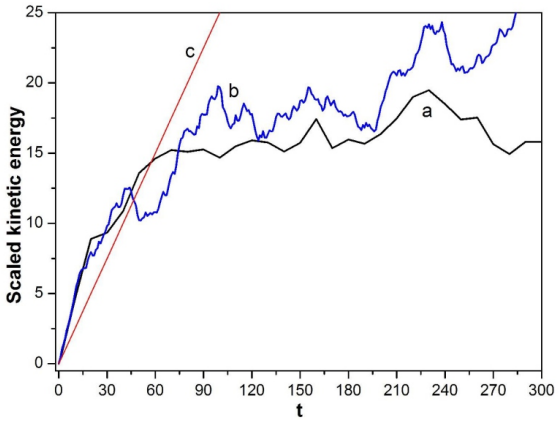

Fig. 12. Scaled kinetic energy in time corresponding to (a) quantum case for $n = 1$, (b) quantum–spinless case for $k' = k + \frac{H}{2}$, and (c) classical case. Other parameters are $k = 10$, $H = 6$, $\tau = 1$, and sign (+). Results are shown up to $t = 300$.

the appropriate spinless evolution operator, i.e., assuming the ordinary QKR with the parameter $k' = k + \frac{H}{2}$. Thus, we emphasize that for $n = 1$, the functions (37) and (38) are in quite satisfactory agreement, while for $n > 1$, the difference becomes bigger and bigger with a further increase in n. For $n = 1$, in the initial t interval the appropriate kinetic energies given by a and b curves (which correspond to (37) and (38), respectively) are in good agreement with the results shown in Fig. 12. However, k' is greater than k, and that is why b curve somewhat overcomes and cuts classical kinetic energy given by c curve, which is also shown in Fig. 12. Thus, a quite good agreement between b and c curves is obtained for the initial values of t. Considering that curve b is a good approximation for curve a, this explains the similarity between the quantum and classical initial growth of the kinetic energy in Figs. 9 and 10.

4. Conclusions

In conclusion, we can say that with the proposed functional form in the kicking potential corresponding to a highly inhomogeneous magnetic field, we have obtained the anomalous and continuous growth of the $\langle \mathrm{LOC} \rangle$ for an increasing value of H. It is more pronounced if the inhomogeneity of the magnetic field is greater. All transfer matrix calculations indicate a polynomial of quadratic degree as the optimal approximation for the $\langle \mathrm{LOC} \rangle$ dependence on H for greater inhomogeneity, which is different from the appropriate well-known behavior for the spinless QKR [26, 27]. In particular, we emphasize that the tight-binding model (24) has also been introduced here. It has been verified by calculating LOC for the quasi-energy states obtained by solving the eigenvalue problem (28).

Further, as a result of the strongly conspicuous inhomogeneity of the magnetic field, quasi-extended states occur. This is also confirmed by calculating the inverse participation ratio depending on inhomogeneity as well as pair-correlations. We emphasize that they could change known characteristics of QKR. For example, some kind of "localization–delocalization" transition appears now. It was shown as well by the following time evolution of the appropriate wave packet in the angular momentum space assuming increasing inhomogeneity. Thus, we emphasize that for extremely large inhomogeneity, dynamical localization is destroyed.

The laser electric field as a "kick" induces an electric dipole moment in the hydrogen-like atom [30]. The accompanying interaction between the induced dipole moment and the electric field gives rise to potential energy, U, for the atom given by

$$U = -\boldsymbol{E} \cdot \vec{\alpha} \boldsymbol{E} = -\boldsymbol{\mu}_{\mathrm{i}} \cdot \boldsymbol{E}, \tag{39}$$

where $\vec{\alpha}$ is the atomic polarizability tensor, $\boldsymbol{E}$ the electric field, and $\boldsymbol{\mu}_{\mathrm{i}}$ the induced dipole moment. Atom shape depends on several factors, including the angular momentum of electrons and the electrostatic forces between atomic particles. Then, assuming that the hydrogen-like atom is not completely spherical, the polarizability tensor is anisotropic. Thus, we will show that the proposed model can serve as an assessment simulator for the induced dipole moment. Furthermore, we assume that the inhomogeneity of the magnetic field in the model is the cause of the anisotropy.

For quasi-energy states, we have

$$\Delta m \, \Delta\theta \gtrsim 1, \tag{40}$$

where $\Delta m \sim 2 \cdot \mathrm{LOC}$, which depends on n and $\min \Delta\theta \sim \epsilon$, where ϵ is small enough. Thus, less LOC indicates greater anisotropy but in the angular momentum space. Otherwise, extended states can be considered there as isotropic. Here, we will assume that ϵ reflects the effect of anisotropy in $\theta-$space so that the following corrected formula is obtained

$$\boldsymbol{\mu}_{\mathrm{i}} \cdot \boldsymbol{E} = \alpha \Big(1 \pm \frac{\epsilon}{2}\Big) E^2, \tag{41}$$

where α is the scalar atomic polarizability and the second term in parentheses is the simplified effect of anisotropy. Higher anisotropy means higher ϵ, and conversely, lower anisotropy means lesser ϵ. In general, assuming a sufficiently large n, for quasi-extended states, $\Delta m \to \infty$ and $\epsilon \to 0$, i.e., there is no more anisotropy. In that case, the comparison can be made with an isotropic noise situation and dynamical localization, can be destroyed [16].

Appendix

Test results for the integral (29) are the following:

1. $n = 1$, $k = 10$, $H = 6$, sign(+), $r = 1$
   Real part $= 0.126336212089194$
   Imag part $= -0.012176923818877$

2. $n = 2$, $k = 10$, $H = 6$, sign(+), $r = 551$
   Real part = 0.000024606756124
   Imag part = 0.000000000000000
3. $n = 3$, $k = 10$ $H = 6$, sign(+), $r = 6$
   Real part = −0.052632923106889
   Imag part = −0.071482397531063

References

[1] F.M. Izrailev, *Phys. Rep.* **196**, 209 (1990).

[2] B. Chirikov, D. Shepelyansky, *Scholarpedia* **3**, 3550 (2008).

[3] S. Fishman, in: *Lecture Notes for the International School of Physics "Enrico Fermi" on Quantum Chaos*, Course CXIX, North-Holland, Amsterdam 1993, p. 187.

[4] F. Haake, *Quantum Signature of Chaos*, Springer-Verlag, Berlin 1991.

[5] M.S. Santhanam, S. Paul, J.B. Kannan, *Phys. Rep.* **956**, 1 (2022).

[6] D.R. Grempel, R.E. Prange, S. Fishman, *Phys. Rev. A* **29**, 1639 (1984).

[7] E. Doron, S. Fishman, *Phys. Rev. Lett.* **60**, 867 (1988).

[8] J. Wang, A.M. García-García, *Phys. Rev. E* **79**, 036206 (2009).

[9] J.-C. Garreau, *Comptes Rendus. Phys.* **18**, 31 (2017).

[10] R. Scharf, *J. Phys. A* **22**, 4223 (1989).

[11] D.R. Mašović, A.R. Tančić, *Phys. Lett. A* **191**, 384 (1994).

[12] D.R. Mašović, *J. Phys. A* **28**, L147 (1995).

[13] R. Blümel, U. Smilansky, *Phys. Rev. Lett.* **69**, 217 (1992).

[14] M. Thaha, R. Blümel, U. Smilansky, *Phys. Rev. E* **48**, 1764 (1993).

[15] F.L. Moore, J.C. Robinson, C.F. Bharucha, B. Sundaram, M.G. Raizen, *Phys. Rev. Lett.* **75**, 4598 (1995).

[16] D.H. White, S.K. Ruddell, M.D. Hoogerland, *New J. Phys.* **16**, 113039 (2014).

[17] J. Chabé, G. Lemarié, B. Grémaud, D. Delande, *Phys. Rev. Lett.* **101**, 255702 (2009).

[18] C. Hainaut, A. Rançon, J.-F. Clément, J.C. Garreau, P. Szriftgiser, R. Chicireanu, D. Delande, *Phys. Rev. A* **97**, 061601(R) (2018).

[19] C. Hainaut, A. Rançon, J.-F. Clément, I. Manai, P. Szriftgiser, D. Delande, J.C. Garreau, R. Chicireanu, *New J. Phys.* **21**, 035008 (2019).

[20] C. Hainaut, I. Manai, J.-F. Clément, J.C. Garreau, P. Szriftgiser, G. Lemarié, N. Cherroret, D. Delande, R. Chicireanu, *Nat. Commun.* **9**, 1382 (2018).

[21] M. Bitter, V. Milner, *Phys. Rev. Lett.* **118**, 034101 (2017).

[22] S. Zhdanovich, C. Bloomquist, J. Floß, I.S. Averbukh, J.W. Hepburn, V. Milner, *Phys. Rev. Lett.* **109**, 043003 (2012).

[23] D.R. Mašović, *J. Phys. A* **54**, 095701 (2021).

[24] M. Abramowitz, I.A. Stegun, *Handbook of Mathematical Functions*, National Bureau of Standards, Washington, D.C. 1968.

[25] G. Casati, L. Molinari, F. Izrailev, *Phys. Rev. Lett.* **64**, 1851 (1990).

[26] D.L. Shepelyansky, *Phys. Rev. Lett.* **56**, 677 (1986).

[27] D.L. Shepelyansky, *Physica D* **28**, 103 (1987).

[28] F. Borgonovi D. Shepelansky, *Europhys. Lett.* **29**, 117 (1995).

[29] D.R. Mašović, *J. Mod. Opt.* **70**, 623 (2023).

[30] D.R. Mašović, *Phys. Lett. A* **375**, 558 (2011).